CLEAVAGE FRACTURE IN A EUTECTOID AND HYPOEUTECTOID STEEL

F. P. L. Kavishe and T. J. Baker*

Cleavage fracture has been studied in steels containing 0.75% and 0.58% C. Specimens for the determination of proof stress, $\sigma_{o.2}$ and cleavage fracture stress, σ_f were heat treated such that the prior austenite grain size remained constant whilst the pearlite interlamellar spacing, S_t was varied. Both σ_f and $\sigma_{o.2}$ increase with decreasing S_t. In coarse pearlite, σ_f increases with decreasing test temperature. In fine pearlite, σ_f is temperature independent. It is concluded that the micromechanisms of cleavage fracture in pearlitic steels depend on strength. In the lower strength condition, cleavage is nucleation-controlled. In the higher strength condition, cleavage is propagation-controlled.

INTRODUCTION

The micromechanism of cleavage fracture in low carbon mild steels appears to be well understood. Cleavage fracture occurs when microcracks formed in brittle carbide particles propagate into the neighbouring ferrite matrix (Smith (1), Knott (2), Curry and Knott (3), Knott (4). The nucleation of the carbide crack is usually attributed to dislocation pile-ups in the ferrite but it has been suggested by Lindley et al (5) that cracking may occur by a fibre loading mechanism. The critical event is the propagation of the microcracks which act as Griffith defects. For this to occur, a critical tensile stress known as the cleavage fracture stress has to be attained. Fracture is propagation-controlled and the cleavage fracture stress is largely dependent on the size of the cracked carbides.

The cleavage fracture stress in mild steels has been shown to be independent of temperature when fracture is induced by slip (2). The yield stress, on the other hand, increases with decreasing test temperature. Such observations have been made on low carbon mild

* Department of Metallurgy and Materials Science, Imperial College, Prince Consort Road, London SW7 2BP, England.

steels but are generally assumed to be relevant to most steels. Thus a temperature independent cleavage fracture stress and a propagation-controlled fracture process has been proposed for bainitic steels (Brozzo et al (7), Curry (8), martensitic steels (Kamada et al (9), Norstrom and Vingsbo (10), Bowen and Knott (11), and fully pearlitic steels (Park and Bernstein (12).

In fully pearlitic steels, it was suggested (12) that crack nucleation occurs by the process of shear cracking proposed by Miller and Smith (13). Dislocation pile-ups in the ferrite impinge on cementite lamellae and cause them to crack. The resultant planar array of microcracks in the cementite undergoes ductile linking to form a larger microcrack which may then propagate as a Griffith defect. The cleavage fracture stress was assumed to be temperature independent to comply with a propagation-controlled mechanism. However, a recent study of cleavage fracture in a fully pearlitic steel by Lewandowski and Thompson (14) has shown that the cleavage fracture stress is temperature independent only in fine pearlitic microstuctures. In coarse pearlite it was found that the cleavage fracture stress increased with decreasing test temperature. Fracture was thought to occur after the attainment of a critical strain or stress-strain product ahead of a crack tip.

The objective of the present research has been to investigate further the process of fracture in a eutectoid steel and to attempt to identify the micromechanism of cleavage fracture in pearlite. It was thought useful, having established the micromechanism of cleavage fracture in pearlite, to extend the study to a hypoeutectoid steel containing a low volume fraction of proeutectoid ferrite.

EXPERIMENTAL TECHNIQUES

The chemical composition (wt. %) of the eutectoid steel was 0.75%C, 0.23%Si, 1.12%Mn, 0.023%P, and 0.026%S. That of the hypoeutectoid steel was 0.58%C, 0.21%Si, 0.75%Mn, 0.031%P and 0.034%S. Test specimens were austenitized for 1 hour at 900 °C and isothermally transformed at temperatures between 510 °C and 650 °C. These heat treatments were designed to produce a constant austenite grain size with a large variation in pearlite interlamellar spacing. Some specimens were also normalised or furnace cooled from 900 °C.

The series ES and HS specimens were used to study the influence of interlamellar spacing on proof stress, $\sigma_{o.2}$ cleavage fracture stress, σ_f and plane strain fracture toughness, K_{IC} in the eutectoid and hypoeutectoid steels respectively. The temperature dependence of $\sigma_{o.2}$ and σ_f was studied using the series EC and HC specimens (coarse pearlite) and series EF (fine pearlite).

Uniaxial proof stresses were determined using either Hounsfield no

13 specimens or compression specimens measuring 3x3x6 mm. Single notched bend (SNB) specimens of the geometry shown in figure 1 were used to determine σ_f. The Griffiths and Owen (6) finite element stress analysis was used to calculate σ_f from the measured fracture loads. The early stages of crack nucleation were studied using double notched bend (DNB) specimens which have been described previously (11),(14). The plane strain fracture toughness was determined according to the procedure described in BS 5447: 1977.

The series ES and HS specimens were tested at −80 and −100 °C respectively. The rest of the specimens were tested in the temperature range −25 to −196 °C. Low temperatures were selected to ensure that the specimens would fracture prior to general yield. Temperatures were maintained to ± 2 °C, and all tests were performed in duplicate.

RESULTS

The effect of interlamellar spacing S_t on the proof stress, cleavage fracture stress and plane strain fracture toughness is shown in table 1. The data for the eutectoid steel are plotted in figure 2 whilst those of the hypoeutectoid steel are plotted in figure 3. It can be seen that both $\sigma_{0.2}$ and σ_f increase with decreasing interlamellar spacing, the effect being more pronounced in the eutectoid steel. The plane strain fracture toughness of the eutectoid steel decreases initially with decreasing interlamellar spacing but increases again for the finest spacing. The effect of interlamellar spacing on K_{IC} in the hypoeutectoid steel is similar to that in the eutectoid steel for pearlite spacings of up to 0.27μm. For the coarsest spacing studied, K_{IC} decreases again.

TABLE 1 - Mechanical properties of the eutectoid steel (−80 °C) and the hypoeutectoid steel (−100 °C, except HR^+ at −80 °C).

Spec.	Trans-formation Temp. °C	Inter-lamellar Spacing μm	Proof Stress MN/m^2	Cleavage Fracture Stress MN/m^2	Fracture Toughness $MN/m^{3/2}$	Ferrite Volume Fraction %
ER	As-received	0.21	573	1406	26.5	< 0.5
ES1	510	0.10	818	1955	28.9	< 0.5
ES2	580	0.19	630	1488	25.1	0.5
ES3	650	0.26	546	1325	29.8	0.8
ES4	1.6 °C/min.	0.33	519	1249	34.5	1.0
HR^+	As-received	0.19	550	1254	43.9	7.8
HS1	510	0.11	665	1546	27.2	1.1
HS2	580	0.19	601	1321	24.9	2.3
HS3	650	0.26	527	1153	32.2	7.2
HS4	1.6 °C/min.	0.31	485	1058	25.2	15.1

The series EC specimens were normalised from 900 °C and had a relatively coarse interlamellar spacing of 0.25 μm. The variation of σ_f and $\sigma_{0.2}$ with test temperature in these specimens is shown in figure 4. It can be seen that the proof stress increases progressively as the test temperature decreases. The notable feature of these results is that σ_f also increases with decreasing testing temperature.

The EF series of specimens were isothermally transformed at 550 °C and had a relatively fine spacing of 0.12 μm. The effect of test temperature on σ_f and $\sigma_{0.2}$ in these specimens is shown in figure 5. The proof stresses are higher than for the EC series which is a consequence of the finer pearlitic spacings, but the temperature dependence of $\sigma_{0.2}$ is very similar. The major difference between the fine and coarse pearlite is that in fine pearlite σ_f is independent of testing temperature.

The temperature dependence of $\sigma_{0.2}$ and σ_f in the hypoeutectoid steel is shown in figure 6 for the HC series of specimens. These specimens were normalised from 900 °C and had a relatively coarse interlamellar spacing of about 0.23 μm. It is of note that the temperature dependence of these specimens is very similar to that shown by the series EC specimens of the eutectoid steel. Both $\sigma_{0.2}$ and σ_f increase with decreasing test temperature.

Figure 7 shows the relationship between $\sigma_{0.2}$ and σ_f in the eutectoid and hypoeutectoid steels. The data includes those obtained from the microstructural conditions described in this paper and others which are reported by the authors elsewhere (16). It appears that for σ_f values less than about 2100 MN/m^2, σ_f is directly proportional to the proof stress, the constant of proportionality being about 2.4. For σ_f values equal to or greater than 2100 MN/m^2, σ_f is largely independent of $\sigma_{0.2}$

FRACTOGRAPHY

All fracture surfaces examined showed that fracture occured by transgranular cleavage. The cleavage facet size scaled with the pearlite nodule size. Examination of fracture surfaces which had been etched in nital revealed that individual facets contained several pearlite colonies. Such groups of colonies are thought to constitute pearlite nodules.

The DNB specimens were loaded in pure bending. Under these conditions the two notches are exposed to nominally identical stress and strain. Usually only one of the notches fails. The unbroken notch then represents the condition of the specimen immediately prior to fracture. If the region beneath the unbroken notch is sectioned and subjected to appropriate metallographic examination, it may be possible to detect non-propagating microcracks.

When DNB specimens were tested, only those with a coarse pearlitic microstructure revealed the presence of microcracks beneath the unbroken notch. The cracks scaled with the colony size, and tended to be oriented at an angle of about 45° to the direction of maximum tensile stress. When examined at high magnification, it was revealed that the microcracks were not continuous but consisted of a series of voids connected by ligaments of plastically deformed ferrite (figure 8).

DISCUSSION

The effects of testing temperature on the cleavage fracture stress suggest that there is a fundamental difference in the micromechanism of cleavage fracture in coarse and fine pearlite. Previous studies of the deformation of pearlite have also indicated different plastic deformation mechanisms for coarse and fine pearlite (17),(18). It is appropriate therefore to consider the two types of microstructure separately.

Coarse pearlite

Langford (17) and Porter et al (18) suggested that the dominant deformation mechanism in coarse pearlite is the formation of localised slip bands which may traverse complete pearlite colonies. Dislocation pile-ups in the ferrite lamellae impinge on the adjacent cementite lamellae and cause them to crack. This deformation is similar to the inhomogeneous slip which causes carbide cracking and the nucleation of cleavage fracture in mild steels (1). The difference between mild steel and coarse pearlite is that in the former the cleavage fracture stress is independent of test temperature, whereas in the latter σ_f increases with decreasing test temperature.

The temperature independence of the cleavage fracture stress in low carbon steels suggests a propagation-controlled cleavage process. A critical tensile stress is required to cause the carbide-initiated crack nucleus to propagate into the neighbouring ferrite matrix. The cleavage fracture stress can then be related to the carbide size by the Griffith equation for a plate-like carbide as follows:

$$\sigma_f = \left[\frac{4E.\gamma_p}{\pi(1-\nu^2)C_o} \right]^{1/2} \qquad \text{- - - - - - - - - (1)}$$

where E is Young's modulus, γ_p is the effective surface energy of ferrite, ν is Poisson's ratio and C_o is the carbide thickness.

Each of the quantities in this equation is relatively insensitive to temperature, and thus σ_f is also temperature insensitive. The fact that σ_f is temperature dependent in coarse pearlite is indicative of a different micromechanism of cleavage fracture.

A cleavage fracture stress for pearlite may be calculated from equation 1 using the known values of the constants and measured values of carbide thickness. The iron carbide lamellae in pearlite are significantly thinner than the carbides found in low carbon mild steels. The average thickness of cementite lamellae in the coarse pearlitic condition was found to be about 0.03 μm. If this value is inserted in equation 1, together with typical values of 207 x 10^3 MN/m^2 for E, 14 J/m^2 for γ_p and 0.3 for ν, the calculated value of σ_f is about 11,600 MN/m^2. This is much larger than the measured values of σ_f for coarse pearlite which were in the range 1507 to 2315 MN/m^2. It follows that if an individual lamellar carbide, or even an array of lamellae was to crack under the influence of an impinging slip band, the resultant microcracks would be too small to cause unstable propagation. The cracks would blunt in the ferrite and remain as a stable array of microcracks. The existence of such an array of stable microcracks prior to the onset of cleavage fracture has been verified and demonstrated using the double notched specimens (figures 8).

The presence of the cracked carbide lamellae as shown in figure 8 encourages plastic deformation to remain concentrated in the original shear band. As a result, the carbide-initiated microvoids can undergo ductile shear linking to form a larger microcrack. This process is the same as that referred to as shear cracking of pearlite (13). When the microcrack attains a critical size, it can then propagate as an unstable cleavage crack. This mechanism implies that cleavage fracture in coarse pearlite is caused by a crack nucleus which is formed by a predominantly fibrous process. This was confirmed when fracture surfaces were studied in the scanning electron microscope. As shown in figure 9, a fibrous fracture facet was found to be located adjacent to the tip of a fatigue pre-cracked specimen. All of the surrounding facets are fully cleavage.

An essential requirement for a propagation-controlled cleavage mechanism is that crack nucleation should be easier than crack propagation. This situation usually exists in the case of mild steels because the surface energy of the brittle carbide is significantly lower than the effective surface energy of the ferrite. If, as is suggested for coarse pearlite, the initial carbide crack is stable, then the subsequent formation of the critical crack nucleus must involve plastic deformation of the ferrite. Under these circumstances, nucleation is more difficult than the subsequent propagation and fracture becomes nucleation-controlled. A triaxial state of stress ahead of the notch root is still necessary in order to provide the high value of tensile stress necessary for crack propagation. Because of the need for continued plastic deformation to develop the enlarged ferrite-plus-carbide crack nucleus, the tensile stress ahead of the notch root is expected to approach the maximum constrained value for yielding before unstable cleavage can occur. This is borne out by the observation that the measured values of cleavage fracture stress for coarse pearlite are all about 2.4 times the uniaxial proof stress.

Coarse pearlite tested at −196 °C

The σ_f values obtained at −196 °C from specimens with a coarse pearlitic microstructure no longer maintained the same relationship with the proof stress as was observed at higher test temperatures. The σ_f values were about 2300 MN/m² which is only about 1.6 times the proof stress. This difference in the degree of constraint from the near constant value of 2.4 at higher temperatures implies a change in the micromechanism of cleavage fracture and may suggest that with the higher stresses available at −196 °C, cleavage becomes propagation-controlled. The measured σ_f value is still less than the calculated value of 11,600 MN/m² for propagation from a single lamellar carbide. This suggests either that propagation occurs preferentially from a particularly large carbide or more probably that the stress fields from a number of adjacent cracked carbides interact to form a larger effective crack size. The important difference from the fracture mechanism proposed for the higher temperature regime is that the crack nucleus is now confined to the carbide particles and hence cleavage can be propagation-controlled.

Fine pearlite

Fine pearlite exhibited σ_f values which were independent of test temperature. As in the case of mild steel, this is indicative of a propagation-controlled cleavage mechanism. Since the thickness of the carbide lamellae in fine pearlite is even smaller than in coarse pearlite, a single cracked carbide lamella cannot be expected to initiate cleavage fracture. However, the mechanism of plastic deformation and carbide cracking in fine pearlite is different from that in coarse pearlite. This may be responsible for the observed difference in cleavage behaviour.

It has been reported (17), (18) that fine pearlite does not exhibit inhomogeneous deformation and does not undergo shear cracking as is predominant in coarse pearlite. The ferrite deforms by fine scale slip and the cementite appears to fail by a fibre loading mechanism. Under these circumstances crack nucleation is expected to occur in a pearlite colony which is aligned parallel to the direction of the maximum principal stress. When a carbide particle fails by a fibre loading mechanism the elastic strain energy in the fibre is released over a distance equal to half the critical fibre length on either side of the fracture (5). The elastic energy released is about an order of magnitude greater than the energy required to form the fracture surface in the carbide. The excess energy is then available to drive the carbide-nucleated microcrack into the ferrite on either side of the carbide lamella. In this way, a crack nucleus can be generated which may be much larger than the thickness of the cracked carbide. An individual crack may be of sufficient size to cause unstable fracture under the influence of the triaxial stress state ahead of the notch root.

Alternatively, the cracking of one cementite lamella may trigger the failure of the similarly stressed cementite lamellae on either side. Such cracking of adjacent carbides in fine pearlite has been observed previously (18). If a number of lamellae were to break simultaneously, the resultant microcrack would be sufficient to permit unstable propagation.

The mechanism proposed for the cleavage fracture of fine pearlite involves a strain-controlled nucleation event, but the critical stage is the propagation of the nucleus which depends on the magnitude of the tensile stress. It follows that cleavage fracture in fine pearlite is propagation-controlled. The cleavage fracture stress is therefore not expected to show a significant variation with testing temperature. This is borne out experimentally both in the present work and elsewhere (14).

The two micromechanisms of cleavage fracture discussed above imply that as the interlamellar spacing is refined, there should be a transition from nucleation-controlled to propagation-controlled cleavage. A similar transition is observed with coarse pearlite when the testing temperature is lowered. Figure 7 shows that the transition from nucleation-controlled to propagation-controlled cleavage fracture occurs at a σ_f value of about 2100 MN/m^2. It may be concluded from the above observations that the micromechanisms of cleavage fracture in pearlite depend on strength. For σ_f values less than about 2100 MN/m^2, the stress required to satisfy the Griffith crack propagation criterion for a single carbide is much larger than the constrained yield stress $m\sigma_{0.2}$ where the constraint factor m is shown in figure 7 to be about 2.4. Since the maximum stress available is limited to the constrained yield stress, the first-formed carbide microcrack is stable and must continue to grow by the failure of both ferrite and cementite lamellae until the critical size is attained to allow propagation. Cleavage fracture under these conditions is therefore nucleation-controlled. For σ_f values greater than or equal to 2100 MN/m^2, unstable propagation can occur from adjacent carbide microcracks and the Griffith propagation stress is less than or equal to 2.4 times the proof stress. This then permits the propagation-controlled mode of cleavage fracture.

The Hypoeutectoid Steel

The σ_f results of the hypoeutectoid steel suggest that the micromechanisms of cleavage fracture are similar in the two steels. In the coarse pearlitic condition, σ_f increased with decreasing temperature (fig. 6) in a similar manner to the eutectoid steel. Also as shown in figure 7, the relationship between σ_f and $\sigma_{0.2}$ is similar. In the lower strength conditions σ_f is proportional to $\sigma_{0.2}$, whereas in the higher strength condition, represented by the data determined at −196 °C, the relationship between σ_f and $\sigma_{0.2}$ is no longer maintained.

Plane strain fracture toughness

The effect of interlamellar spacing on K_{IC} is shown in figure 2 for the eutectoid steel. As the spacing decreases, K_{IC} first decreases and then increases for the finest spacings. A similar influence of interlamellar spacing on K_{IC} has been reported by Preston (20). The minimum value in the K_{IC} curve was observed at an interlamellar spacing of about 0.16 μm. The variation in K_{IC} reflects the effect of interlamellar spacing on the deformation of pearlite and is likely to be related to the change in the micromechanism of cleavage fracture.

The effect of interlamellar spacing on K_{IC} in the hypoeutectoid steel is shown in figure 3 and appears to be similar to that observed in the eutectoid steel for pearlite spacings up to about 0.27 μm. At the spacing of 0.31 μm, a lower K_{IC} was obtained. This value was associated with specimen HS4 in table 1 which had a relatively high volume fraction of proeutectoid ferrite (15.1%). All the other specimens had less than 8% ferrite by volume. The relatively low K_{IC} value may be attributed to the high ferrite content of specimen HS4.

CONCLUSIONS

It is concluded that the micromechanisms of cleavage fracture in pearlitic steels depend on the microstructure and strength of the steel. In lower strength conditions associated with coarse pearlite, cleavage fracture is nucleation-controlled and involves the nucleation of a microcrack by fibrous cracking of the pearlite. Unstable cleavage occurs when the microcrack attains a critical size due to the failure of successive ferrite and cementite lamellae.

In higher strength conditions cleavage fracture is propagation controlled. Fracture occurs when carbide microcracks undergo unstable propagation. The transition from nucleation-controlled to propagation-controlled cleavage fracture may be achieved either by a reduction in interlamellar spacing or by a reduction in testing temperature. The change in the micromechanism of fracture brought about by changes in interlamellar spacing is reflected in the fracture toughness K_{IC}.

SYMBOLS USED

K_{IC} = plane strain fracture toughness

σ_f = cleavage fracture stress

$\sigma_{0.2}$ = proof stress

S_t = true interlamellar spacing of pearlite

REFERENCES

(1) Smith, E., in Proceedings of Conf. "Physical Basis of Yield and Fracture", Oxford, England, 1966, pp. 36, The Institute of Phys. and Phys. Society.

(2) Knott, J. F., J. Iron and Steel Inst., Vol. 204, 1966, pp. 104.

(3) Curry, D. A. and Knott, J. F., Metal Science, Vol. 12 November 1978, pp. 511.

(4) Knott, J. F., "Fundamentals of Fracture Mechanics", Butterworths, London, England, 1973.

(5) Lindley, T. C., Oates, G. and Richards, C. E., Acta Metallurgica, Vol. 18, 1970, pp. 1127.

(6) Griffiths, J. R. and Owen, D. R. J., J. Mech. Phys. Solids, Vol. 19, 1971, pp. 419.

(7) Brozzo, P., Buzzichelli, G., Mascanzoni, A. and Mirabile, M., Metal Science, Vol. 11, 1977, pp. 123.

(8) Curry, D. A., Metal Science, Vol. 18, 1984, pp. 67.

(9) Kamada, A., Koshizuku, N. and Funakoshi, T., Trans. Iron and Steel Inst. of Japan, Vol. 16, 1976, pp. 407.

(10) Norstrom, L. A. and Vingsbo, O., Metal Science, Vol. 13, 1979, pp. 677.

(11) Bowen, P. and Knott, J. F., Metal Science, Vol. 18, 1984, pp. 225.

(12) Park, Y. J. and Bernstein, I. M., in "Rail Steels–Development, Processing and Use", ASTM STP 644. Edited by D. H. Stone and G. G. Knupp, ASTM, Philadelphia, Pa, USA, 1978, pp. 287.

(13) Miller, L. E. and Smith, G. C., J. Iron and Steel Inst., Vol. 208, 1970, pp. 998.

(14) Lewandowski, J. J. and Thompson A. W., in "Proc. 6th Int. Conf. on Fracture", New Delhi, India. Edited by S. R. Valluri et al, 1984, pp. 1515.

(15) Underwood, E. E., "Quantitative Stereology", Addison-Wesley, Reading, Massachusetts, USA, 1970, pp. 73.

(16) Kavishe, F. P. L. and Baker, T. J., "The effect of prior austenite grain size and pearlite interlamellar spacing on the strength and fracture toughness of a eutectoid rail steel", Materials Science and Technology, London, 1985, (in press).

(17) Langford, G., Metall. Trans., Vol. 8A, 1977, pp. 861.

(18) Porter, D., Easterling, K. and Smith, G., Acta Metallurgica, Vol. 26, 1978, pp. 1405.

(19) Lindbourg, U., Trans. ASM, Vol. 61, 1968, pp. 500.

(20) Preston, R. R., "Wear resistant materials in the steel industry", The Metallurgist and Materials Technologist, The Inst. of Metallurgists, London, England, Dec. 1980, pp. 687.

ACKNOWLEDGEMENTS

Many thanks are due to the Swiss Development Cooperation for their financial support of one of the authors (FPLK), the British Steel Corporation who provided the steels and to Professor D. W. Pashley, FRS, for providing the research facilities.

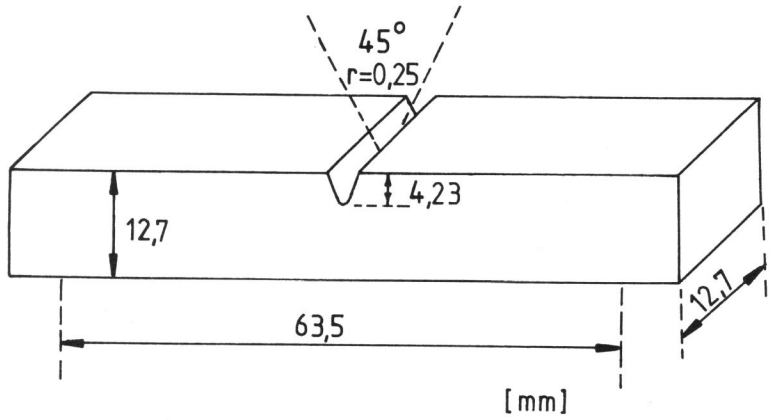

FIGURE 1 Dimensions of the bend specimen

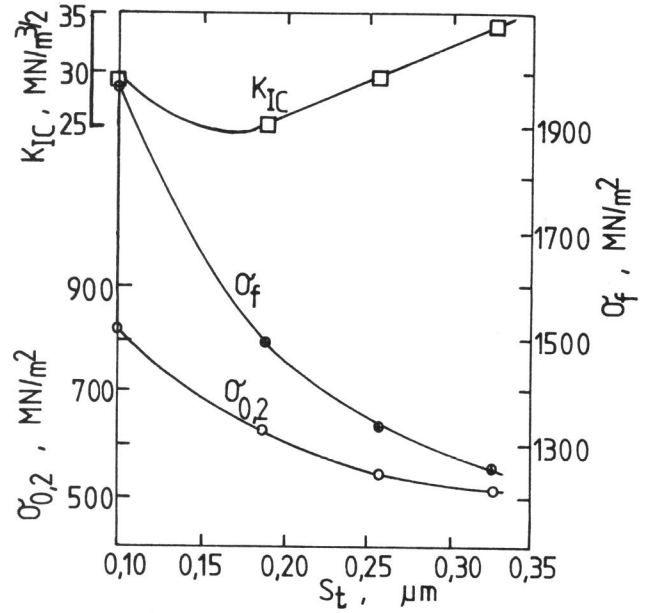

FIGURE 2 Dependence of proof stress, cleavage fracture stress and K_{IC} on interlamellar spacing

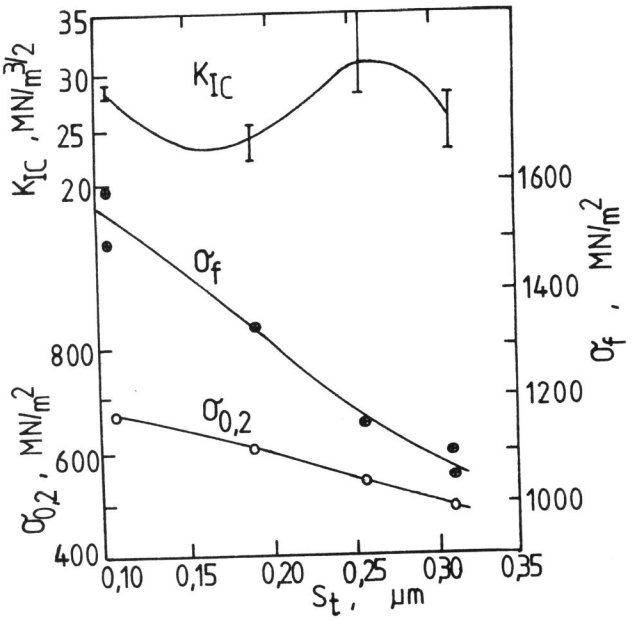

FIGURE 3 Dependence of proof stress, cleavage fracture stress and K_{IC} on interlamellar spacing

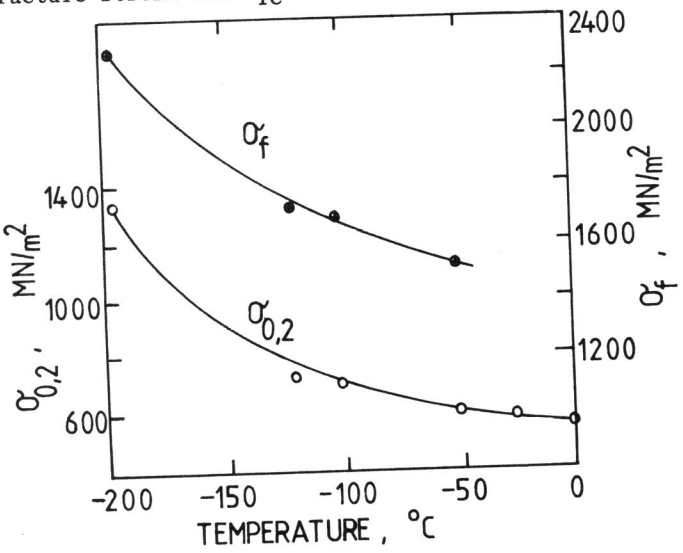

FIGURE 4 Effect of test temperature on proof stress and cleavage fracture stress (eutectoid)

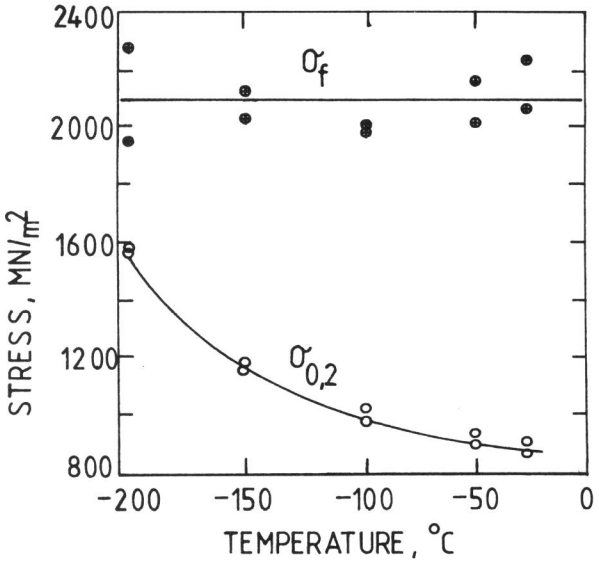

FIGURE 5 Effect of test temperature on proof stress and cleavage fracture stress (eutectoid)

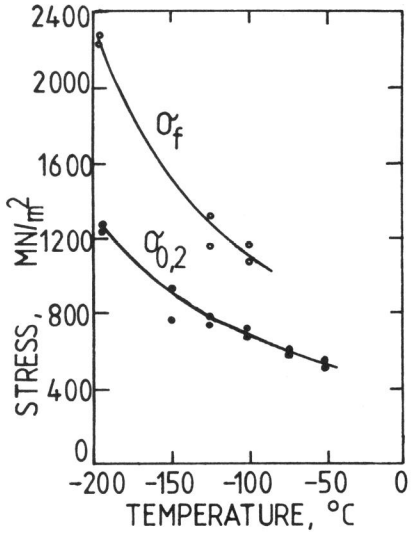

FIGURE 6 Effect of temperature on proof and fracture stresses

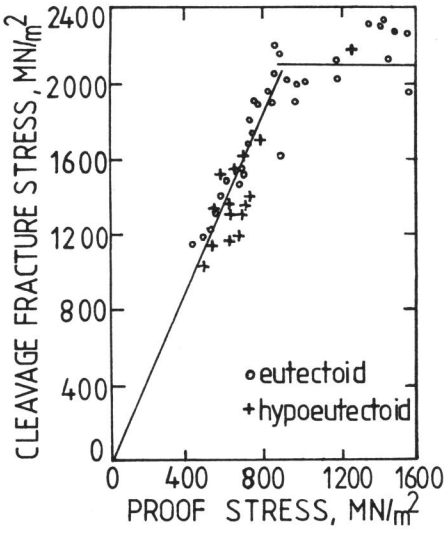

FIGURE 7 Relationship between $\sigma_{0.2}$ and σ_f in the two steels

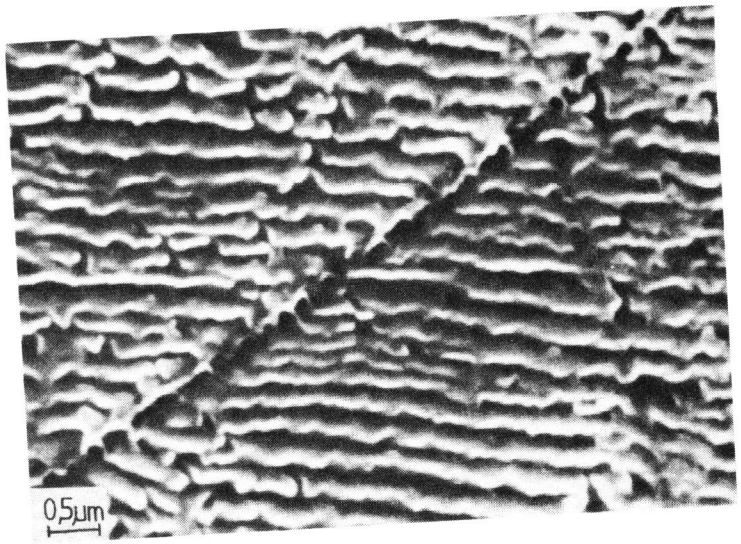

FIGURE 8 The non-propagating microcrack seen below the notch root of a DNB specimen

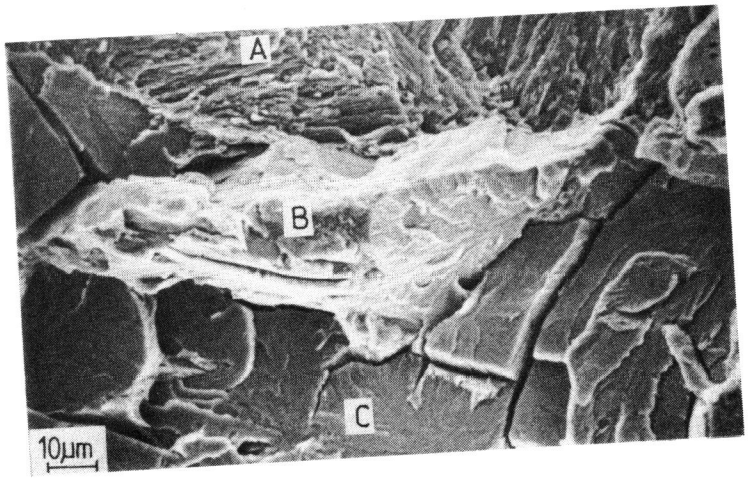

FIGURE 9 A fibrous fracture facet (B) adjacent to the tip of a fatigue crack (A). Area (C) is cleavage